Actuated Dynamic Walking in a Seven-Link Biped Robot

David J. Braun, *Member, IEEE*, Jason E. Mitchell, and Michael Goldfarb, *Member, IEEE*

***Abstract*—The authors have previously described a method for enabling fully actuated biped walking without prescribing joint angle trajectories or imposing kinematic constraints between joints. This method was hypothesized to offer a more natural-looking bipedal gait and a higher locomotive efficiency relative to methods requiring accurate joint trajectory tracking. In this paper, the authors present experimental evidence to support both hypotheses. Specifically, the authors describe the design of a seven-link bipedal robot appropriate for the previously proposed control method; present the implementation of the "nonkinematic" control approach on the biped robot; demonstrate (with data, photographic sequences, and video) the "relaxed" style of walking resulting from the control method; and experimentally characterize the locomotive efficiency of the biped in terms of the mechanical cost of transport. The latter results are compared to corresponding measures reported elsewhere in the literature.**

***Index Terms*—Actuated dynamic walking, biped robot, biped walking, robot control and design.**

I. Introduction

MANY approaches have been formulated for the control of bipedal locomotion, see [1] for a recent review. One of the best established of these is the zero-moment-point (ZMP) approach, introduced by Vukobratović and Stepanenko [2], [3]. The ZMP approach ensures balance during walking by computing and tracking joint trajectories such that the sum of all resultant forces on the biped can be reacted through the support polygon between the robot and ground. By utilizing this approach, numerous methods have been proposed for walking control and stable pattern formation [4]–[6]. Application of ZMP-based methods have been shown to provide effective, robust, and versatile locomotion for biped robots [7]–[9]. However, such methods typically require accurate tracking of joint trajectories, which in turn require high joint output impedances. This gives the robot the appearance of a "stiff" looking unnatural gait, characterized by a low locomotive efficiency [10], relative to humans. The former is due to the high joint output impedance required to accurately track the joint angle trajectories (see [11] for the related discussion, and possible resolution), and the latter is presumably due to the fact that trajectory tracking requires a reshaping of the inertial and gravitational dynamics of the robot, which, in turn, can be energetically expensive. By contrast, humans (which are characterized by natural looking gait with high locomotive efficiency) have been shown to leverage the natural dynamics of their limbs when walking (e.g., [12]).

Rather than enforce joint trajectories via servocontrol, other researchers have developed bipedal walking machines that maintain a stable gait with a minimum amount of joint control authority. Specifically, fully passive dynamic walkers rely on precisely tuned natural dynamics of the biped, and must walk on a slight downward slope to be powered by gravity. Examples of these types of walkers are described by [13]–[15]. Actuator-assisted dynamic walkers augment a nearly passive walker by introducing a reduced set of actuators to overcome the energetic losses associated with gait (i.e., the walkers need not descend a slope) and to introduce some robustness to design parameter variation (via some form of feedback control). Examples of actuator-assisted walkers are described in [16]–[18]. Such approaches are characterized by a low joint output impedance and an improvement in locomotive efficiency, relative to joint trajectory tracking methods [10], [16]. Such approaches, however, are typically underactuated, and thus, less capable and less robust relative to fully actuated joint trajectory control approaches.

The authors have described in a recent paper a method for enabling fully actuated biped robot walking without prescribing joint angle trajectories or imposing kinematic constraints between joints [19], i.e., the described approach can be used to generate a stable limit cycle without prescribing or accurately tracking kinematic trajectories or enforcing kinematic constraints. Instead, the described method utilizes state-dependent control torques (generated by low-gain spring–damper couples) to provide coordination of the motion without specifying the response of the system. The joint behavior is, therefore, characterized by low output impedance, such that the motion of the biped results from the combined influences of the prescribed joint torques and the gravitational and inertial dynamics of the robot (as opposed to being dictated via trajectory tracking).

Pratt *et al*. [20] also presented a method that need not override the natural dynamics of the biped (depending on the choice of control parameters). However, unlike in [20], the method incorporated herein relaxes all assumptions regarding robot

Manuscript received March 1, 2010; revised June 16, 2010, August 8, 2010, and October 20, 2010; accepted October 21, 2010. Date of publication December 30, 2010; date of current version January 9, 2012. Recommended by Technical Editor J. Ueda.

D. J. Braun is with the School of Informatics Edinburgh, University of Edinburgh, Edinburgh, EH8 9AB, U.K. (e-mail: david.braun@ed.ac.uk, david.braun@vanderbilt.edu).

J. E. Mitchell and M. Goldfarb are with the Department of Mechanical Engineering, Vanderbilt University, Nashville, TN 37235 USA (e-mail: jason.mitchell@vanderbilt.edu; michael.goldfarb@vanderbilt.edu).

This paper has supplementary downloadable material available at http://ieeexplore.ieee.org. provided by the authors. The material includes a video, Dynamic Walking Experiment.wmv, which demonstrates *actuated dynamic walking* of a seven-link anthropomorphic biped robot. The video can be played with Windows Media Player. The total size is 13.28 MB. Contact david.braun@vanderbilt.edu for further questions about this work.

Color versions of one or more of the figures in this paper are available online at http://ieeexplore.ieee.org.

Digital Object Identifier 10.1109/TMECH.2010.2090891

configuration (i.e., feet need not be flat on the ground) imposes state-dependent torques generated by low-gain spring–damper couples, which are constructed as strictly passive functions with fixed equilibrium points; references some of these torques to an inertial reference frame and others to the internal robot frame; and develops a model-based solution to transform the state-dependent control torques to actuator joint torques.

It was hypothesized in [19] that, since the described approach incorporates rather than overrides the inertial characteristics of the robot and corresponding gravitational influences, the resulting gait would offer improved energy efficiency and a more "natural-looking" and "relaxed" appearance, relative to approaches that require accurate joint trajectory tracking (which are referred to herein as "kinematic" approaches). These hypotheses were supported in [19] with numerical simulations of the walking controller on a seven-link biped robot with human-like inertial and geometric properties.

This paper describes the design and construction of a seven-link biped robot appropriate for implementation of the fully actuated, nonkinematic walking approach (i.e., the approach requires backdrivable joints, such that power can flow from the joint to the actuator, as well to from the actuator to the joint). The description of the robot design is followed by a description of the implementation of the proposed controller on the seven-link robot. Finally, experimental results and an accompanying video supplement demonstrate stable bipedal walking synthesized with the proposed control method. The mechanical cost of transport is characterized and compared to corresponding efficiency measures reported for other biped robots in the literature.

II. Model of the Biped

A brief overview of the control framework proposed in [19] is presented here to describe the control law for the nonkinematic walking method, to define controller parameters for the experimental implementation, and to motivate the real-time sensing requirements for the biped robot design.

Since the control method is model-based, we first introduce the biped model. Fig. 1 presents the geometric structure of the seven-link robot. The configuration of the biped is defined with nine coordinates, $\mathbf{q} = [x, y, \theta, \theta_1, \theta_2, \theta_3, \theta_4, \theta_5, \theta_6]^T$, where the first two coordinates represent the translational motion of the robot in the inertial frame, while the last seven angular coordinates reference the orientation of the links with respect to the inertial frame. In order to support the forthcoming analysis, we will also define the joint angles (relative angles between the links) as: $\boldsymbol{\varphi} = [\varphi_1, \varphi_2, \varphi_3, \varphi_4, \varphi_5, \varphi_6]^T = [\theta_1 - \theta, \theta_2 - \theta_1, \theta_3 - \theta_2 + \pi/2, \theta_4 - \theta, \theta_5 - \theta_4, \theta_6 - \theta_5 + \pi/2]^T$. The biped is actuated at each joint (i.e., right and left hip, knee, and ankle joints), such that the dynamics of the robot are affected by six actuator torques, $\mathbf{u} = [u_1, u_2, u_3, u_4, u_5, u_6]^T$, which are considered positive in the same (counterclockwise) direction as the joint angles.

In the following, we consider the biped to be a constrained mechanical system [21]. By means of this framework, the model of the biped can be represented with a constrained equation of motion in every motion phase [19]. In the present paper, we will only present the basic elements of such a model which provides the necessary information for the closed-loop control design. These elements are the differential equations of the flight phase motion, and the (algebraic and differential) relations which define the kinematic (physical) constraints during the motion.

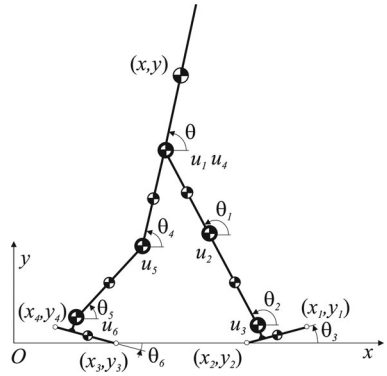

Fig. 1. Seven-link biped with the absolute coordinates $\mathbf{q}$ and the control torques $\mathbf{u}$. The Cartesian coordinates $(x_i, y_i), i \in \{1, 2, 3, 4\}$, represent the position of the toe and the heel for the left and right leg.

A. Unconstrained Dynamics

The equations of motion for the 9-DoF (unconstrained) "flying" biped, can be written as

$$\mathbf{M}(\mathbf{q})\ddot{\mathbf{q}} + \mathbf{h}(\mathbf{q}, \dot{\mathbf{q}}) + \mathbf{G}(\mathbf{q}) = \mathbf{Q}_u \tag{1}$$

where $\mathbf{M} \in \Re^{9\times 9}$ is a symmetric and positive definite mass matrix, $\mathbf{h} \in \Re^9$ represents the inertial forces, $\mathbf{G} \in \Re^9$ represents the gravitational forces, while $\mathbf{Q}_u = \mathbf{E}\mathbf{u}$ is a generalized control force computed using a constant matrix $\mathbf{E} \in \Re^{9\times 6}$ which maps the control inputs $\mathbf{u} \in \Re^6$ to the generalized control force space.

B. Kinematic Constraints

For the biped in Fig. 1, neither foot can penetrate the ground, the knee joints cannot extend beyond the fully straight position, and both feet are assumed not to slide when in contact with the ground. Since each toe and heel is independently characterized by nonpenetration and nonslip with the ground, the flight phase dynamics (1) can be subject to the following kinematic (physical) constraints:

$$\boldsymbol{\Phi}_h(\mathbf{q}) = \begin{bmatrix} y_1 \\ y_2 \\ y_3 \\ y_4 \\ \varphi_2 \\ \varphi_5 \end{bmatrix} = \mathbf{0}, \qquad \boldsymbol{\Phi}_n(\mathbf{q}, \dot{\mathbf{q}}) = \begin{bmatrix} \dot{x}_1 \\ \dot{x}_2 \\ \dot{x}_3 \\ \dot{x}_4 \end{bmatrix} = \mathbf{0} \tag{2}$$

where $(x_i, y_i), i \in \{1, 2, 3, 4\}$ are the toe and heel coordinates (see Fig. 1), while $\varphi_2 = \theta_2 - \theta_1$ and $\varphi_5 = \theta_5 - \theta_4$ are the relative angles at the knee joint. Instead of using (2) directly, the controller requires only the following information:

$$\mathbf{A}(\mathbf{q}) = [(\partial \boldsymbol{\Phi}_h / \partial \mathbf{q})^T, (\partial \boldsymbol{\Phi}_n / \partial \dot{\mathbf{q}})^T]^T. \tag{3}$$

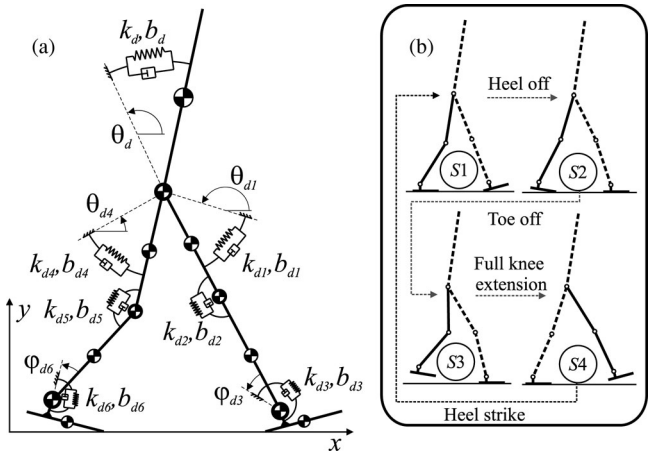

Fig. 2. (a) Control elements and the control parameters on a seven-link robot. (b) Configuration-based switching logic with the four separate states: $S1$—stance, $S2$—push-off, $S3$—swing, and $S4$—late swing. The particular state flow, $S1 \rightarrow S2 \rightarrow S3 \rightarrow S4 \rightarrow S1 \ldots$, together with the corresponding switching events, which correspond to normal walking, is indicated with dashed lines.

Depending on the configuration of the robot, the constraints concatenated in (2) and (3) are active when they restrict the motion and inactive when they do not. In order to ensure that $\mathbf{A}$ only contains the active constraints, the configuration of the robot is monitored through the motion to identify and eliminate the inactive constraints by zeroing the corresponding row in (3). The constraint matrix obtained in this way carries the kinematic information from the configuration of the biped for use in the control law.

III. Control Approach

In this section, we recall the basic elements of the control law for actuated dynamic walking recently developed by the authors [19]. The control approach can be considered in two parts. First, low-impedance generalized forces are prescribed to encourage a walking pattern, and second these generalized forces are mapped to joint torques as described in Section III-B.

A. Generalized Control Forces

In order to generate patterned movement without requiring accurate trajectory tracking or imposing kinematic constraints (such as symmetry), the seven link robot is provided with seven control elements which are spring–damper couples with fixed equilibrium points (see Fig. 2). Each control element is characterized by three control parameters: a stiffness constant, a damping constant, and an equilibrium angle. These parameters are changed as piecewise constant functions through four separate states as the biped walks, using a configuration-based switching controller.

1) Computing the Generalized Control Forces: For a given set of control parameters, the desired generalized control force is computed as

$$\mathbf{Q}_d = -\mathbf{K}_d(\boldsymbol{\phi} - \boldsymbol{\phi}_d) - \mathbf{B}_d\dot{\boldsymbol{\phi}} \tag{4}$$

where $\boldsymbol{\phi} = [\theta, \theta_1, \varphi_2, \varphi_3, \theta_4, \varphi_5, \varphi_6]^T$ is obtained by position feedback, $\dot{\boldsymbol{\phi}}$ is known from the corresponding velocity feedback, while the control parameters concatenated in the stiffness matrix,

$$\mathbf{K}_d = \begin{bmatrix} 0 & 0 & 0 & 0 & 0 & 0 & 0 \\ 0 & 0 & 0 & 0 & 0 & 0 & 0 \\ k_d & 0 & 0 & 0 & 0 & 0 & 0 \\ 0 & k_{d1} & -k_{d2} & 0 & 0 & 0 & 0 \\ 0 & 0 & k_{d2} & -k_{d3} & 0 & 0 & 0 \\ 0 & 0 & 0 & k_{d3} & 0 & 0 & 0 \\ 0 & 0 & 0 & 0 & k_{d4} & -k_{d5} & 0 \\ 0 & 0 & 0 & 0 & 0 & k_{d5} & -k_{d6} \\ 0 & 0 & 0 & 0 & 0 & 0 & k_{d6} \end{bmatrix}$$

damping matrix,

$$\mathbf{B}_d = \begin{bmatrix} 0 & 0 & 0 & 0 & 0 & 0 & 0 \\ 0 & 0 & 0 & 0 & 0 & 0 & 0 \\ b_d & 0 & 0 & 0 & 0 & 0 & 0 \\ 0 & b_{d1} & -b_{d2} & 0 & 0 & 0 & 0 \\ 0 & 0 & b_{d2} & -b_{d3} & 0 & 0 & 0 \\ 0 & 0 & 0 & b_{d3} & 0 & 0 & 0 \\ 0 & 0 & 0 & 0 & b_{d4} & -b_{d5} & 0 \\ 0 & 0 & 0 & 0 & 0 & b_{d5} & -b_{d6} \\ 0 & 0 & 0 & 0 & 0 & 0 & b_{d6} \end{bmatrix}$$

and the equilibrium angles $\boldsymbol{\phi}_d = [\theta_d, \theta_{d1}, 0, \varphi_{d3}, \theta_{d4}, 0, \varphi_{d6}]^T$ are assigned by the configuration-based switching controller as discussed in the next two sections.

Before we proceed further, let us point out that while (4) has the same form as a usual PD control law, the philosophy and the application of (4) are entirely different. Specifically, we use piecewise constant (fixed) equilibrium angles $\boldsymbol{\phi}_d$ instead of tracking a predefined desired trajectory $\boldsymbol{\phi}_d = \boldsymbol{\phi}_d(t)$. While this difference may not seem crucial, one can recognize that contrary to the precise trajectory tracking that requires high-gain PD control, the fixed angular references (see Fig. 2) make high gains not well suited to walking control. Accordingly, utilization of low control gains is not only a preference to generate compliant motion, but also a requirement for stable gait synthesis. An alternative compliant motor control strategy for anthropomorphic robots was recently proposed in [22].

2) State-Dependent Control: In order to achieve a walking motion, the control parameters are selected depending on the configuration of the robot. In this light, we define four separate states for each leg depending on whether the toe and/or the heel touch the ground and whether the leg is fully extended at the knee joint (see Fig. 2). In each state, the logic assigns three control parameters for each of the seven control elements from a set of user-defined desired parameters. Parameter selection can be guided as follows.

3) Generalized Force Parameter Selection: During walking, one of the primary objectives is to keep the upper body in an upright vertical position. Utilizing the control elements which act between the body and the inertial reference frame, one can set the stiffness parameter and the equilibrium angle to provide a near upright position for the body, and then use the associated damping parameter to influence the body dynamics. A similar

idea can be used to generate leg oscillation (with respect to a fixed inertial reference) by using the control elements attached to the thigh. Specifically, in swing, a low stiffness and low damping element pulls the leg towards a fixed hip flexion configuration (specified with an equilibrium angle), while in the stance phase, a higher stiffness and higher damping is assigned to the same control element which encourages the stance leg to move towards a fixed hip extension angular configuration. The knee stiffness and damping is also modulated, by using a relatively high value in stance (to support the body with the help of the knee hyperextension stop), and employing only slight damping during swing phase to generate (partially) ballistic swing. Ankle impedance parameters are tuned by mimicking the strategy taken by humans. Accordingly, the ankle stiffness is used to accumulate elastic energy from middle stance phase and to deliver energy by altering the equilibrium angle during push-off. The main control parameter at the swinging ankle is an equilibrium point which should be adjusted to provide slight dorsiflexion, to avoid stumbling and scuffing during swing.

B. Actuator Torques

The control influences specified by $\mathbf{Q}_d$ cannot be directly imparted to the walking robot. Rather, the robot can only be effected by the joint torques, $\mathbf{u}$. The control approach described herein computes the joint torque vector $\mathbf{u}$ that provides either the same motion that would result from the generalized force vector $\mathbf{Q}_d$, or if the same motion is not possible, the approach computes the joint torque vector that minimizes the acceleration energy between the desired and the realizable motion. This solution is given as follows.

Since we are interested in control of the constrained motion, let us recall here the acceleration component of the constrained motion generated by the desired generalized control forces

$$\ddot{\mathbf{q}}_d = \mathbf{R}^{-1}\mathbf{N}\mathbf{R}^{-T}\mathbf{Q}_d \tag{5}$$

where $\mathbf{R}$ is the upper triangular Cholesky factorization of the mass matrix $\mathbf{M} = \mathbf{R}^T\mathbf{R}$ (where $\mathbf{M}$ is defined in (1)), $\mathbf{N} = \mathbf{I} - (\mathbf{A}\mathbf{R}^{-1})^+(\mathbf{A}\mathbf{R}^{-1})$ is the null-space projection operator of the inertially weighted constraint matrix (where $\mathbf{A}$ is defined by (3)). Using the above relation, one can also define the constraint consistent accelerations generated with the actuator torques

$$\ddot{\mathbf{q}}_u = \mathbf{R}^{-1}\mathbf{N}\mathbf{R}^{-T}\mathbf{E}\mathbf{u}. \tag{6}$$

Following the main objective $\ddot{\mathbf{q}}_d = \ddot{\mathbf{q}}_u$, one could equate (5) and (6) and solve the corresponding linear equation for $\mathbf{u}$. Depending on the constraint configuration of the robot however, this solution may not exist (in cases when the robot is underactuated, for example, in flying phase or if only one toe or one heel is contacting the ground). In order to obtain an approximate solution even when the robot is underactuated, we propose not to solve $\mathbf{u}$ from $\ddot{\mathbf{q}}_d = \ddot{\mathbf{q}}_u$ directly, but rather to define a solution which minimizes the acceleration energy between the desired and the real motion $(\ddot{\mathbf{q}}_d - \ddot{\mathbf{q}}_u)^T\mathbf{M}(\ddot{\mathbf{q}}_d - \ddot{\mathbf{q}}_u) \rightarrow \min$. The particular solution to this problem is given with

$$\mathbf{u} = (\mathbf{N}\mathbf{R}^{-T}\mathbf{E})^+\mathbf{N}\mathbf{R}^{-T}\mathbf{Q}_d \tag{7}$$

where $(*)^+$ is a Moore-Penrose generalized inverse (pseudoinverse) of $(*)$ [23]. Note that whenever the control computation is redundant, (7) provides a solution by also minimizing the squared Euclidean norm of the joint torques [19], [24].

Let us point out here that (7) defines a full-body control law where each joint torque depends on the motion of the robot. It is also important to recognize that no inverse dynamics is performed to cancel the gravitational and inertial forces along the motion and enforce a predefined reference trajectory on the system. Instead, the natural (inertial and gravitational) dynamics of the robot are allowed to substantially influence the motion of the biped, which is synthesized using low-impedance joint torques which encourage but do not dictate patterned motion. As subsequently demonstrated, the described approach allows emulation of a human-like walking of a seven-link biped robot.

IV. Seven-Link Biped Robot Design

The fully actuated, nonkinematic walking approach described by (4) and (7) was implemented on a seven-link biped robot. In order to avoid suppression of the inertial and gravitational dynamics of the biped, the robot was designed with low-output impedance (i.e., backdrivable) joints, such that power could flow relatively unimpeded through the biped joints from the actuators to the environment, and from the environment to back to the actuators. The resulting biped robot, shown in Fig. 3, is 1.2 m tall and has a total mass of 14.3 kg. The geometric parameters and mass distribution of the robot are given in Table I. The seven links of the robot are the upper body and right and left thigh, shank, and foot segments, respectively. The robot incorporates six joint actuators, which are right and left hip, knee, and ankle actuators, respectively. The biped is constrained to walk in a circular path of 1.6 m radius by a mechanical tether attached at the hip joint, as shown in Fig. 9 and in the video supplement. Note that a set of ball bearings between the mechanical tether and the robot prevents any significant moment from being transferred from the tether to the robot in the plane of walking. Let us also mention that, as shown in Fig. 9, the mechanical tether is loosely connected to a vertical mast through a slack cable. The cable does not contribute any support forces to the robot while walking, but rather will prevent the robot from collapsing fully in the case that the robot trips or stumbles. Finally, note that the mechanical tether is used only to constrain the motion of the robot to the plane, but is neither instrumented nor used to provide a rotational position reference for measuring body orientation. In the following sections, we discuss joint actuation, foot design, upper body characteristics, and the sensory system implemented for walking control [25].

A. Upper Body

The upper body of the robot carries 4.54 kg (10 lb) of weights, distanced 0.2 m from the hip joint (see Fig. 3), which provide an inertial approximation of a head, arms, and trunk. The body includes a single-axis gyroscope (Analog Devices, ADXR150), which directly measures its sagittal plane angular velocity with respect to the inertial reference frame. The sensor is characterized with $\pm 150^\circ/\mathrm{s}$ measurement range and a noise density

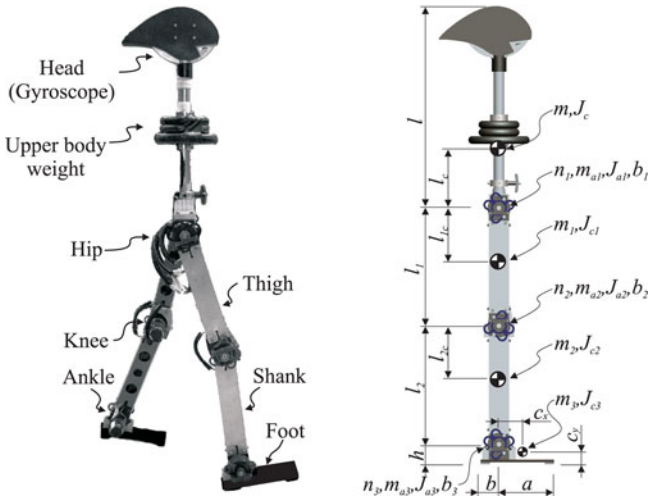

Fig. 3. (Left) Experimental prototype of the seven-link dynamic walker developed at Vanderbilt University, Center for Intelligent Mechatronics. (Right) CAD model, side view of the seven-link biped. The values for the model parameters are reported in Table I; specifically, the table lists the geometric parameters, the link masses m, m_1, m_2, m_3, link moments of inertias for the center of mass $J_c, J_{c1}, J_{c2}, J_{c3}$; actuator masses m_{a1}, m_{a2}, m_{a3}, actuator moments of inertias J_{a1}, J_{a2}, J_{a3}, the gear ratios on the reducers on the joints $n_1 : 1, n_2 : 1, n_3 : 1$, and the experimentally identified joint level linear viscous damping constant b_1, b_2, b_3.

TABLE I
GEOMETRIC AND INERTIAL PARAMETERS OF THE ROBOT DEPICTED IN FIG. 3 WITH TOTAL MASS OF $M = 14.3$ KG AND HEIGHT OF $L = 1.2m$

Structure	no. $(*)$	l_* $[m]$	l_{c*} $[m]$	m_* $[kg]$	J_{c*} $[kgm^2]$
Body	–	0.390	0.185	6.12	0.021
Thigh	1	0.295	0.147	0.67	0.0096
Shank	2	0.298	0.14	0.55	0.0069
Foot	3	0.183	–	0.36	0.0007
Foot	$a[m]$	$b[m]$	$h[m]$	$c_x[m]$	$c_y[m]$
	0.137	0.046	0.055	0.014	0.035
Actuators	no. $(*)$	n_*	$m_{a*}[kg]$	$J_{a*}[kgm^2]$	$b_*[Nms]$
Hip	1	21	0.84	0.0067	≈ 0.13
Knee	2	12	0.84	0.0022	≈ 0.11
Ankle	3	21	0.84	0.0067	≈ 0.05

of $0.05^\circ/\mathrm{s}/\sqrt{\mathrm{Hz}}$. In order to reduce the noise level, the analog signal is filtered with a first-order low-pass filter with a 50-Hz roll-off frequency.

B. Actuation

All joint actuation units consist of the same essential structure, with slight modifications in gear ratio and range of motion. A representative joint actuation unit (for the knee) is shown in Fig. 4. Each unit consists of a 150 W brushed dc motor (Maxon RE40), which drives the respective joint through a low gear ratio planetary reducer (Maxon GP42C), specifically 21:1, 12:1, and 21:1 for the hip, knee, and ankle units, respectively. The relatively low gear ratio provides sufficient joint torque, while also providing highly backdrivable joint behavior. Demonstration of the passive joint behavior is shown in Fig. 6 and also shown in the supplemental video that accompanies this paper.

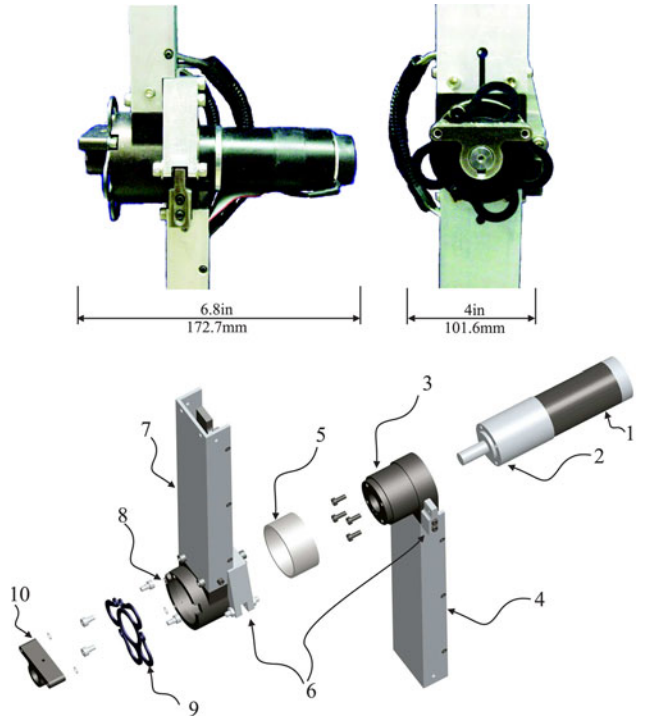

Fig. 4. (Top) Knee joint on the robot, side and frontal views. (Bottom) CAD model—exploded view of the knee joint: 1) encoder; 2) actuation unit—motor and the gearhead; 3) inner bearing housing; 4) lower leg; 5) Teflon sleeve bearing; 6) hard stop at full knee extension; 7) upper leg; 8) external bearing housing; 9) elastic coupling; 10) connecting element.

C. Sensing

The control method (4) and (7) requires knowledge of the postural configuration and constraint condition of the biped. The related information (i.e., rotational coordinates, toe and/or heel contact for each foot and knowledge of full knee extension) are provided by a combination of six joint encoders (one integrated into each joint motor), a MEMS gyroscope mounted on the upper body segment, and force sensing resistors integrated into each foot, as discussed in the following sections.

1) Joint Encoders: Each joint includes an incremental quadrature encoder (Maxon, ENC-MR-L-1024CPT) mounted onto each joint motor (see Fig. 4). The reference position for each of the six encoders is identified in a static stance phase during initialization using two accelerometers (Analog Devices, ADXL203) located on the upper body and the upper right leg, which detect alignment of these links with the gravity vector. The remaining link angles are aligned at initialization using the knee hyperextension stops, and assuming the floor is perpendicular to the gravity vector. The implemented sensors provide an accurate joint angle, φ, measurement which can be characterized with an encoder resolution of $4.2^\circ \times 10^{-3}$ at the hip and ankle joints and $7.3^\circ \times 10^{-3}$ for the knee joints.

2) Foot Design and the Foot Sensors: Each foot is constructed from ABS plastic and instrumented with four force sensing resistors (Interlink, 402 FSR), two on each toe and heel. These sensors are located between the underside of the foot and a thin foot plate made from spring steel (see Fig. 5). When

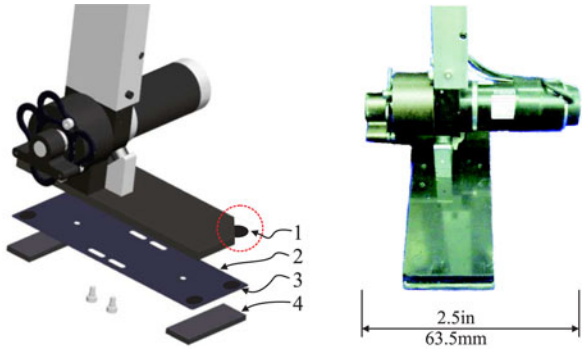

Fig. 5. (Left) CAD model—exploded view of the foot: 1) FSR sensor; 2) foot plate; 3) sensor touch pad; 4) rubber foot contact-pad. (Right) Foot of the robot.

the toe and/or heel touches the ground, the circular rubber pad (located on the foot plate) imparts the resulting force to the foot sensors. The corresponding signal serves to identify the contact configuration between the foot and the ground. Near to the toe and the heel (which are the expected contact areas), the foot-plate is supplemented with silicon rubber pads with high frictional properties, good abrasive durability and appropriate shock absorbing capability. In the proposed control implementation, measurements of the contact forces or moments are not required. As such, the feet are not equipped with load cells.

V. Controller Parameterization and Implementation

In the following, we discuss the implementation of the walking controller. Specifically, we discuss: 1) measurement of generalized coordinate vector required to implement (4) and (7); 2) parameterization of the model for the implementation of (7); 3) experimental validation of the model parameters; and 4) selection of the desired generalized control forces required for the implementation of (4).

A. Measurement of Generalized Coordinates

In the control laws (4) and (7), we utilize both the joint angles $\boldsymbol{\varphi}$ (which are measured by encoders), and also absolute link angles $\boldsymbol{\theta} = [\theta, \theta_1, \theta_2, \theta_3, \theta_4, \theta_5, \theta_6]^T$. Although the absolute orientations are not measured directly, they can be calculated by $\boldsymbol{\theta} = [\theta, \theta + \varphi_1, \theta + \varphi_1 + \varphi_2, \theta + \varphi_1 + \varphi_2 + \varphi_3 - \pi/2, \theta + \varphi_4, \theta + \varphi_4 + \varphi_5, \theta + \varphi_4 + \varphi_5 + \varphi_6 - \pi/2]^T$ if the upper body angle θ is provided. Accordingly, in the following discussion, we will only describe how to compute θ. Once the angular configuration is known, the velocity information is obtained by numerical differentiation. Note that the angle θ could be measured by introducing an angular position sensor between the mechanical tether and the robot; such an implementation, however, would not be realizable once the mechanical tether is removed, and thus the authors chose instead to implement measurement of the upper body angle in a manner that would translate directly to generalized (i.e., 3-D) walking.

1) Computing the Absolute Orientation of the Upper Body: Whenever the robot is not underactuated (at least one foot is flat on the ground or, either the backward toe or heel and the forward toe or heel is on the ground), the system has 6 or less DoFs, and the absolute angular orientation for the upper body can be calculated using the six encoder measurements $\boldsymbol{\varphi}$ formally stated as

$$\theta = \theta(\boldsymbol{\varphi}). \tag{8}$$

The related kinematic computation is performed exactly if either of the feet touches the ground in two contact points. Otherwise, if the foot touches the ground in three or more contacting points, the upper body angle is solved in a least squares sense to accommodate the kinematic redundancy and mitigate slight measurement errors.

2) Estimating the Absolute Orientation: There are two cases when (8) cannot be applied: if the robot moves through an underactuated configuration (i.e., flight phase or if only one toe or one heel is contacting the ground), or if (8) is singular or nearly singular. Under these conditions, we utilize the gyroscope located on the upper body to directly provide the angular velocity of the upper body, $\dot{\theta} = \dot{\theta}_g$, and estimate the absolute orientation of the upper body θ by

$$\theta = \theta(t_0) + \int_{t_0}^{t} \dot{\theta}_g(\tau) d\tau \tag{9}$$

where $t \in [t_0, t_1), t_0$ is the time instant starting from which (8) cannot be used, while t_1 is the time when (8) can again be used reliably. The interval $[t_0, t_1)$ for which the integration is performed is expected to be short (at most 10% of the step duration), such that the integration drift was not an implementation issue. Instead of employing the presented strategy, a sophisticated inertial measurement unit could also be used to directly provide the upper body velocity and angle continuously in time [26].

Concatenation of (8) and (9) allows reconstruction of the angular motion of the robot in the inertial frame, $\boldsymbol{\theta}$. Note that switching between the two computational schemes could induce discontinuities on position and also on the velocity signals; however, such discontinuities were avoided in the implementation here by numerically blending the two solutions in a short time window after the switching instant.

B. Model Parameterization and Validation

In order to compute (7), the model parameters $\mathbf{E}$, $\mathbf{A}$, and $\mathbf{M}$ are required. The constant matrix $\mathbf{E}$ is known by the actuator arrangement on the robot. The geometric and inertial parameters for each link of the robot (see Table I) were used to compute $\mathbf{A}$ and $\mathbf{M}$, and were estimated by a combination of physical measurements and numerical calculation from the CAD model. The following experiments and simulations were performed with these model parameters.

1) Demonstrating Backdrivability Via Free Swing Experiments: In order to demonstrate backdrivability of the joints (and validate parameter estimation), unactuated experiments were conducted by releasing a given link from a nonvertical initial position, and matching the unforced experimental response with a model-based simulation. The resulting responses for both the experiments and simulations are depicted in Fig. 6, demonstrate that the joints are highly backdrivable. Also, the close match between the experimental and the simulation data

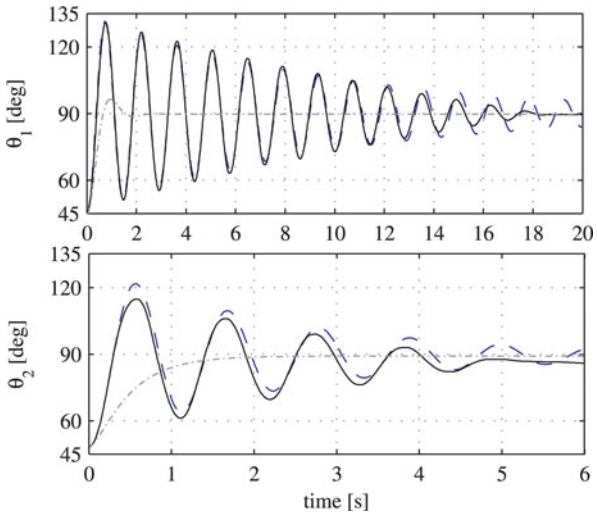

Fig. 6. Free swing experiments, which characterize the passive (uncontrolled) dynamics of the hip and the knee joint. The motion of the device is depicted with (black) solid line, while the simulated response is plotted with dashed (blue) lines. The difference in the low velocity area is mainly due to the Coulomb friction and the cabling which is neglected in the simulations, (the asymmetric effect of the cabling can be seen in the knee response). In order to show the difference between a backdrivable actuator unit utilized here, and a usual highly geared joint design, the dotted (gray) lines depict the model prediction of corresponding motion the robot would have with 105:1 and 60:1 gear ratio on the hip and knee respectively. Due to the low inertia of the foot, a similar free swing experiment is recognized not well suited to characterize the dynamics of the ankle joint, and as such is not conducted here.

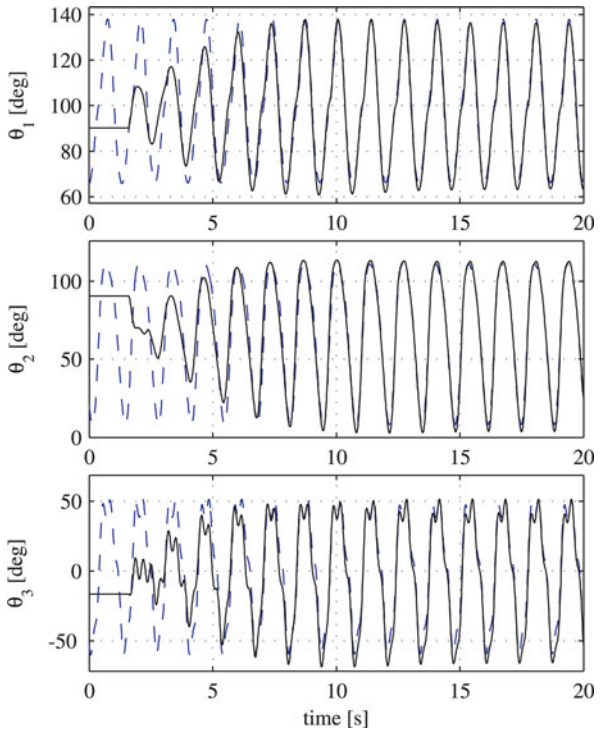

Fig. 7. Low-gain PD control experiment. Solid line (black) represents the motion of the device, while the dashed line (blue) is the corresponding model response. The experiment is performed by applying a control torque vector $\mathbf{u} = -\mathbf{K}_d(\boldsymbol{\varphi} - \boldsymbol{\varphi}_d) - \mathbf{B}_d\dot{\boldsymbol{\varphi}}, \mathbf{K}_d = [2,\ 1.5,\ 1,\ 0,\ 0,\ 0]^T$, $\mathbf{B}_d = [0.2, 0.2, 0.1, 0, 0, 0]^T$, $\boldsymbol{\varphi}_d = [(\pi/3)\sin(1.5\pi t) + \pi/20, (\pi/6)\sin(3\pi t - \pi/2) - \pi/2, (\pi/6)\sin(6\pi t) + \pi/6]^T$.

validates parameter estimation. A video corresponding to the figure is included in the supplemental material.

2) Parameter Validation Via PD Control Experiments: In order to further validate model parameter estimates, a forced response experiment was conducted, using a low-gain PD controller with a periodically modulated equilibrium point. The experimental response and the model prediction are both depicted in Fig. 7, while the corresponding video is given in the supplemental material. Note that using low-gain PD control allows us to validate both the implementation of the actuator unit and the model parameters, namely, the response of the system in this case is not fully prescribed by the control force but rather substantially influenced by the natural dynamics of the robot.

C. Selection of the Control Parameters

As proposed in [19], the state-dependent generalized control force vector depends on user-defined control parameters. As noted in that paper, some type of automated (optimization based) procedure could be formulated to select the control parameters, although such an approach is nontrivial, given the complex, high dimensional, nonlinear, and nonsmooth nature of the problem. However, the parameters (i.e., stiffness, damping, and an equilibrium point) have a clear and direct physical interpretation, and based on the authors experience, these parameters can be determined using the guidance described previously in Section III-A3. Using such guidance, the parameters were initially tuned in a numerical simulation of the biped (such as that described in [19]), and subsequently, iteratively tuned during experimental implementation to provide a stable, yet "relaxed" gait cycle. The resulting parameter sets are listed in Table II.

TABLE II
CONTROLLER PARAMETERS: $k_{d()}$ [N·m], $b_{d()}$ [N·m·s], $\theta_{d()}$ [IN DEGREES]; S1—STANCE, S2—PUSH-OFF, S3—SWING, S4—LATE SWING (SEE FIG. 2)

States	k_d	$k_{d1,4}$	$k_{d2,5}$	$k_{d3,6}$
S1	32	80	6	0
S2	32	15	6	40
S3	32	15	0.5	10
S4	32	0	6	10
	b_d	$b_{d1,4}$	$b_{d2,5}$	$b_{d3,6}$
S1	0.75	4.9	1	1.25
S2	0.75	0.6	1	1.25
S3	0.75	0.6	0.05	0.5
S4	0.75	1.2	1	0.5
	θ_d	$\theta_{d1,4}$	$\varphi_{d3,6}$	
S1	87.5	82	$-(0)$	
S2	87.5	128	-10	
S3	87.5	128	10	
S4	87.5	$-(0)$	0	

The simulation and experimental results (presented in Section VI) are similar, but not exact enough to allow direct transfer of the control parameters without tuning. Probably the most significant difference between the two is that the experimental robot walked in a circle of a fairly small diameter, which introduced 1) considerable energy loss in turning the feet while on the ground, and 2) a mechanical boom which can significantly alter the dynamics of the system. Due to these reasons, and the fact that no reference trajectory is used to enforce a

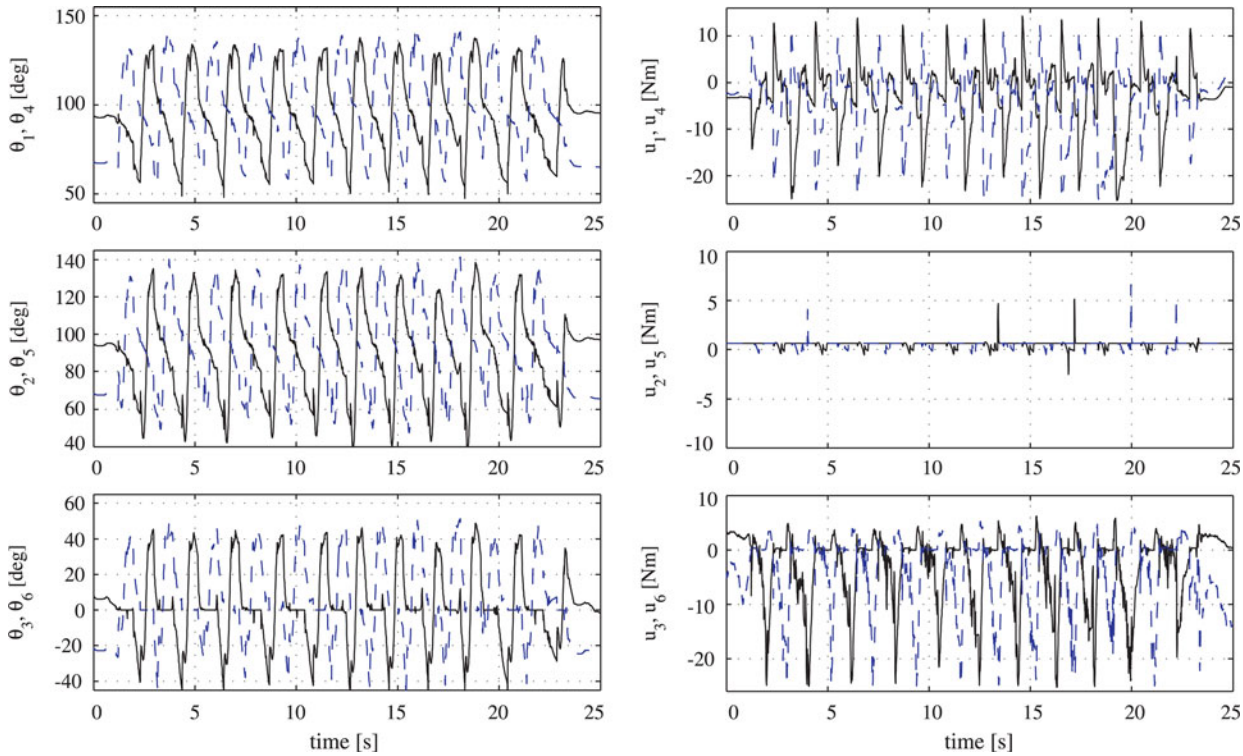

Fig. 8. Actuated dynamic walking—angular data and joint torques. Black/blue (full/dashed) lines depict the motion of the right/left leg. (During the experiment, a small positive constant torque was applied to the knees at single support when locked, which sets a threshold for them to go unlocked.)

desired common motion between the two systems, comparison between simulation and experimental results is recognized not to provide additional insight.

VI. Implementation of the Walking Controller

The controller [see (4) and (7)] with the parameters listed in Tables I and II was implemented on the previously described seven-link biped robot with the real-time environment provided by MATLAB Real-Time Workshop. Note that computation of $\mathbf{A}(\boldsymbol{\theta})$ and $\mathbf{M}(\boldsymbol{\theta})$ requires only the angular configuration of the robot (i.e., computation of (x, y) is not required). Computation implementation of the control law (7) required two standard routines, Cholesky factorization and pseudoinversion, and ran on an Intel Core 2 Quad 2.4-GHz desktop computer at a sampling rate of 1000 Hz.

The walking that resulted from the control parameter set Table II is shown in the data (see Fig. 8), the frame sequence shown in Fig. 9, and in the supplemental video that accompanies this paper. The resultant walking is characterized with an average forward speed of $v_{\text{avg}} \approx 0.5$ m/s, an average step length of $L_{\text{step}} \approx 0.5$ m, and an average stepping frequency of $f_{\text{step}} \approx 1$ Hz.

The presented robot walks with extended knee stance support similar to that realized on passive and actuator assisted dynamic walkers [13], [16], [17]. While such a motion style is recognized to be (energetically) beneficial compared to a usual bent knee robot walking, it is also known to be different than human walking [18]. Like humans, however, our biped has a flat foot and actuated ankles which is employed in a recognizable, human-like way during the walking motion. Specifically, the robot utilized a characteristic rolling foot double-support phase, and a preemptive ankle push-off to propel itself forward. This preemptive ankle push-off, frequently attributed as foot rotation, is known to be utilized by humans, [27], its energetic benefit theoretically justified in [28], and numerically demonstrated during walking and running in [6], [29], and [30]. The extended knee (compass-like) gait leads us to assume that the vertical ground reaction force for our robot resembles a bell shape profile known for passive (point foot) dynamic walking. Due to the human-like ankle actuation, however, such force profile may also contain spikes from a characteristic M-shape profile known for natural human walking [31], [32].

As previously mentioned, the proposed nonkinematic control method was hypothesized to provide improved walking efficiency relative to approaches that require accurate joint trajectory tracking, and was also hypothesized to provide a more "relaxed and natural looking" gait. Regarding the former, the mechanical cost of transport (as proposed in [33]), $c_{\text{mt}} = |\text{mechanical energy}|/(\text{weight} \times \text{distance traveled})$, was measured to be $c_{\text{mt}} \approx 0.31$. By comparison, Collins *et al.*. [16] estimated that the actuator assisted Cornell biped has a $c_{\text{mt}} \approx 0.055$ (similar to the estimate for humans), while the fully actuated, ZMP-based Honda Asimo robot was estimated (in [16]) to be $c_{\text{mt}} \approx 1.6$. Although these numbers cannot be used to directly compare the three robots (due to the lack of dynamic similarity, total number of degrees of freedom, and level of autonomy), they support the hypothesis that nonkinematic control approaches can provide improved locomotive efficiency, relative to approaches that utilize accurate joint trajectory tracking.

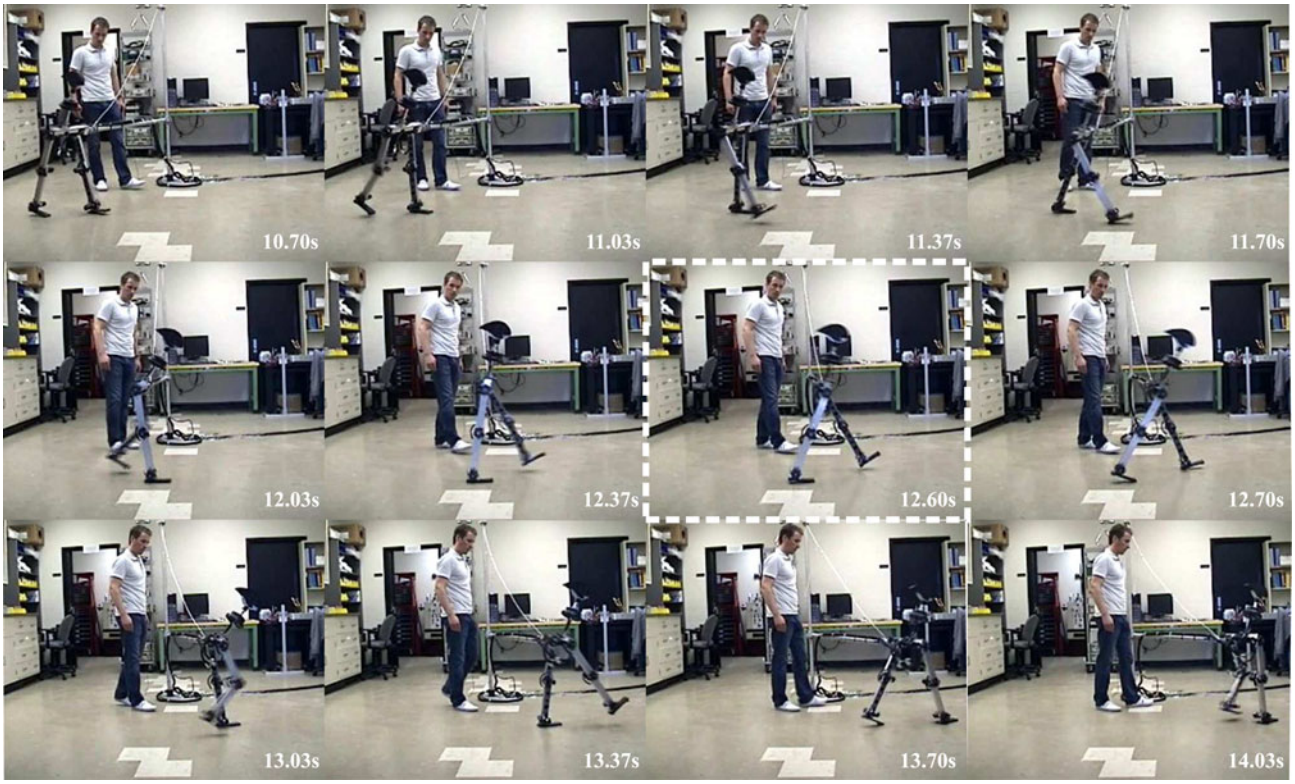

Fig. 9. Actuated dynamic walking—frame sequence extracted from the experimental video. The motion frame marked with dashed white line depicts the preemptive ankle push phase when only the toe on the rear foot is on the ground.

The present force level (spring-like) control does not enforce but only encourages the motion of the biped. Such motion results from the combined influences of the prescribed joint torques and the gravitational and inertial dynamics of the robot (as opposed to being dictated via trajectory tracking). This allowed us to realize a bipedal locomotion where the motion of the robot is not predefined but instead is established by the controlled system itself autonomously. As predicted by the second hypothesis, such a nonkinematic walking approach demonstrated herein appears more relaxed and natural than usual approaches that require accurate joint trajectory tracking. However, the notion of "relaxed" or "natural looking" walking is not easily *quantitatively* assessed. That being said, it is left to the reader to view the supplemental video of walking that accompanies this paper to provide an independent assessment.

VII. Conclusion

The authors have previously presented a "nonkinematic" walking controller (i.e., one that does not prescribe joint trajectories, does not impose kinematic constraints between joints or require symmetry of motion, and does not require accurate joint trajectory tracking), and had in a previous publication hypothesized and shown via numerical simulation that the proposed walking controller would offer improved walking efficiency and a more natural-looking gait. In this paper, the authors described the design of a seven-link biped robot appropriate for implementation of the nonkinematic controller, and describe the implementation of the nonkinematic controller on this robot. The authors present experimental results that support the previously made hypotheses that the controller provides improved locomotive efficiency and a more natural-looking walk relative to control approaches requiring accurate trajectory tracking.

Acknowledgment

This work was conducted during D. J. Braun's Ph.D. research at the Center for Intelligent Mechatronics, Vanderbilt University.

References

[1] Y. Hurmuzlu, F. Génot, and B. Brogliato, "Modeling, stability and control of biped robots—A general framework," *Automatica*, vol. 40, no. 10, pp. 1647–1664, 2004.
[2] M. Vukobratović and J. Stepanenko, "On the stability of anthropometric systems," *Math. Biosci.*, vol. 15, no. 1, pp. 1–37, 1972.
[3] M. Vukobratović, B. Borovac, D. Šurla, and D. Stokić, *Biped Locomotion*. New York: Springer-Verlag, 1990.
[4] Q. Huang, K. Yokoi, S. Kajita, K. Kaneko, H. Arai, N. Koyachi, and K. Tanie, "Planning walking patterns for a biped robot," *IEEE Trans. Robot. Autom.*, vol. 17, no. 3, pp. 208–289, Jun. 2001.
[5] Q. Huang and Y. Nakamura, "Sensory reflex control for humanoid walking," *IEEE Trans. Robot.*, vol. 21, no. 5, pp. 977–984, Oct. 2005.
[6] C. Chevallereau, D. Djoudi, and J. W. Grizzle, "Stable bipedal walking with foot rotation through direct regulation of the zero moment point," *IEEE Trans. Robot.*, vol. 24, no. 2, pp. 390–401, Apr. 2008.
[7] A. Takanishi, M. Ishida, Y. Yamazaki, and I. Kato, "The realization of dynamic walking by the biped walking robot WL-10RD," in *Proc. Int. Conf. Advanced Robot.*, 1985, pp. 459–466.
[8] K. Hirai, M. Hirose, Y. Haikawa, and T. Takenaka, "The development of Honda humanoid robot," in *Proc. 1998 IEEE ICRA*, pp. 1321–1326.
[9] L. Löffler, M. Gienger, and F. Pfeiffer, "Sensors and control concept of walking "Johnnie"," *Int. J. Robot. Res.*, vol. 22, pp. 229–239, 2003.

[10] A. D. Kuo, "Choosing your steps carefully," *IEEE Robot. Autom. Mag.*, vol. 14, no. 2, pp. 18–29, Jun. 2007.
[11] K. Mitobe, G. Capi, and Y. Nasu, "Control of walking robots based on manipulation of the zero moment point," *Robotica*, vol. 18, no. 6, pp. 651–657, 2000.
[12] S. Mochon and T. A. McMahon, "Ballistic walking: An improved model," *Math. Biosci.*, vol. 52, pp. 241–260, 1980.
[13] T. McGeer, "Passive dynamic walking," *Int. J. Robot. Res.*, vol. 9, no. 2, pp. 62–82, 1990.
[14] M. J. Coleman and A. Ruina, "An uncontrolled walking toy that cannot stand still," *Phys. Rev. Lett.*, vol. 80, no. 16, pp. 3658–3661, 1998.
[15] M. Garcia, A. Ruina, A. Chatterjee, and M. Coleman, "The simplest walking model: Stability, complexity, and scaling," *J. Biomech. Eng.*, vol. 120, no. 2, pp. 281–288, 1998.
[16] S. Collins, A. Ruina, R. Tedrake, and M. Wisse, "Efficient bipedal robots based on passive dynamic walkers," *Sci. Mag.*, vol. 307, pp. 1082–1085, 2005.
[17] M. Wisse, G. Feliksdal, J. van Frankenhuyzen, and B. Moyer, "Passive-based walking robot: Denis a simple efficient and lightweight biped," *IEEE Robot. Autom. Mag.*, vol. 14, no. 2, pp. 52–62, Jun. 2007.
[18] F. Iida, Y. Minekawa, J. Rummel, and A. Seyfarth, "Toward a human-like biped robot with compliant legs," *Robot. Auton. Syst.*, 2008.
[19] D. J. Braun and M. Goldfarb, "A control approach for actuated dynamic walking in biped robots," *IEEE Trans. Robot.*, vol. 25, no. 6, pp. 1292–1303, Dec. 2009.
[20] J. Pratt, C. M. Chew, A. Torres, P. Dilworth, and G. Pratt, "Virtual model control: An intuitive approach for bipedal locomotion," *Int. J. Robot. Res.*, vol. 20, pp. 129–143, 2001.
[21] D. J. Braun and M. Goldfarb, "Eliminating constraint drift in the numerical simulation of constrained dynamical systems," *Comput. Methods Appl. Mech. Eng.*, vol. 198, no. 37-40, pp. 3151–3160, 2009.
[22] S.-H. Hyon, "A motor control strategy with virtual musculoskeletal system for compliant antropomorphic robots," *IEEE Trans. Mechatron.*, vol. 14, no. 6, pp. 677–688, Dec. 2009.
[23] A. Ben-Israel and T. N. E. Greville, *Generalized Inverse: Theory and Applications*. Berlin, Germany: Springer, 2003.
[24] D. J. Braun and M. Goldfarb, "A controller for dynamic walking in bipedal robots," in *Proc. 2009 IEEE/RSJ Int. Conf. Intell. Robots Syst.*, St. Louis, MO, Oct. 11–15, pp. 2916–2921.
[25] D. J. Braun, J. E. Mitchell, and M. Goldfarb, "Actuated dynamic walking in biped robots: Control approach, robot design and experimental validation," in *Proc. 9th IEEE-RAS Int. Conf. Hum. Robots*, Paris, France, Dec. 7–10, 2009, pp. 237–242.
[26] S. Lohmeier, T. Buschmann, and H. Ulbrich, "System design and control of anthropomorphic walking robot LOLA," *IEEE Trans. Mechatron.*, vol. 14, no. 6, pp. 658–666, Dec. 2009.
[27] A. Goswami, "Postural stability of biped robots and the foot-rotation indicator (fri) point," *Int. J. Robot. Res.*, vol. 18, pp. 523–533, 1999.
[28] A. D. Kuo, "Energetics of actively powered locomotion using the simplest walking model," *J. Biomech. Eng.*, vol. 124, pp. 113–120, 2002.
[29] D. Tlalolini, C. Chevallereau, and Y. Aoustin. (2010, Mar.). "Human-like walking: Optimal motion of a bipedal robot with toe-rotation motion," *IEEE Trans. Mechatronics,* [Online]. Available: http://ieeexplore.ieee.org, DOI: 10.1109/TMECH.2010.2042458.
[30] G. Schultz and K. Mombaur, "Modeling and optimal control of human-like running," *IEEE Trans. Mechatron.*, vol. 15, no. 5, pp. 783–792, Oct. 2010.
[31] T. S. Keller, A. M. Weisberger, J. L. Ray, S. S. Hasan, R. G. Shiavi, and D. M. Spengler, "Relationship between vertical ground reaction force and speed during walking, slow jogging, and running," *Clin. Biomech.*, vol. 11, no. 5, pp. 253–259, 1996.
[32] H. Geyer, A. Seyfarth, and R. Blickhan, "Compliant leg behaviour explains basic dynamics of walking and running," *Proc. R. Soc. Lond.* B, vol. 273, no. 1603, pp. 2861–2867, 2006.
[33] G. Gabrielli and T. von Kármán, "What price speed?: Specific power required for propulsion of vehicles," *Mech. Eng.*, vol. 72, no. 10, pp. 775–781, 1950.

David J. Braun (M'10) received the B.S. and M.S. degrees in mechanical engineering from the Faculty of Technical Sciences, University of Novi Sad, Novi Sad, Serbia, in 2001 and 2003, respectively, and the Ph.D. degree in mechanical engineering from Vanderbilt University, Nashville, TN, in 2009.

He was a Research Associate at Vanderbilt University. In 2010, he joined the University of Edinburgh, Edinburgh, U.K., where he is currently a Postdoctoral Research Fellow. His research interests include modeling, simulation, and control of dynamical systems with application to walking robots.

Jason E. Mitchell received the B.S. degree from Tennessee Technological University, Cookeville, in 1999, and the M.S. degree from Vanderbilt University, Nashville, TN, in 2002, both in mechanical engineering.

He is currently an Engineer in the Department of Mechanical Engineering, Vanderbilt University. His current research interests include design and fabrication of upper and lower extremity prostheses and robotic walkers.

Michael Goldfarb (M'94) received the B.S. degree in mechanical engineering from the University of Arizona, Tucson, in 1988, and the S.M. and Ph.D. degrees in mechanical engineering from the Massachusetts Institute of Technology, Cambridge, in 1992 and 1994, respectively.

In 1994, he joined the Department of Mechanical Engineering, Vanderbilt University, Nashville, TN, where he is currently the H. Fort Flowers Professor of Mechanical Engineering. His current research interests include the design and control of high power density actuators, control of fluid-powered actuators, the design and control of upper and lower extremity prostheses, restoration of gait to paralyzed persons, and control of bipedal locomotion.